Original Article

Melittin acupoint injection in attenuating bone erosion in collagen-induced arthritis mice via inhibition of the RANKL/NF-κB signaling pathway

Fenfang Liu[1#], Fen Chen[1#], Le Yang[1], Fucheng Qiu[2], Guangen Zhong[3], Shan Gao[1], Weizhe Xi[1], Meilian Lai[1], Qiting He[1], Ying Chen[3], Weiming Chen[3], Jiping Zhang[1*], Lu Yang[1,3*]

[1]School of Traditional Chinese Medicine, Southern Medical University, Guangzhou, China; [2]Intensive Care Unit, Foshan Hospital of TCM, Foshan, China; [3]Department of Acupuncture and Rehabilitation, Integrated Hospital of Traditional Chinese Medicine, Southern Medical University, Guangzhou, China

Contributions: (I) Conception and design: F Liu, F Chen; (II) Administrative support: L Yang, F Qiu; (III) Provision of study materials or patients: G Zhong, S Gao, Y Chen; (IV) Collection and assembly of data: W Xi, M Lai, Q He; (V) Data analysis and interpretation: J Zhang, W Chen; (VI) Manuscript writing: All authors; (VII) Final approval of manuscript: All authors.

[#]These authors contributed equally to this work and should be considered as co-first authors.

[*]These authors contributed equally to this work as co-corresponding authors.

Correspondence to: Jiping Zhang, MM. School of Traditional Chinese Medicine, Southern Medical University, 1023 Shatai South Road, Baiyun District, Guangzhou 510515, China. Email: zhangjp611@163.com; Lu Yang, MD. School of Traditional Chinese Medicine, Southern Medical University, 1023 Shatai South Road, Baiyun District, Guangzhou 510515, China; Department of Acupuncture and Rehabilitation, Integrated Hospital of Traditional Chinese Medicine, Southern Medical University, Yard 13, Shiliugang Road, Haizhu District, Guangzhou 510330, China. Email: yl800526@163.com.

Background: Rheumatoid arthritis (RA) is an autoimmune disease leading to chronic joint inflammation. Bone erosion is the most serious pathological condition of RA and the main cause of joint deformities and disability. Melittin acupoint injection (MAI) is an effective traditional Chinese medicine (TCM) method for RA treatment. This study aimed to investigate the effect of MAI on RA bone erosion and to elucidate the underlying mechanism.

Methods: A collagen-induced arthritis (CIA) mouse model was established as the experimental subject. MAI was administrated once every other day for 28 days to mice with CIA. The effects of MAI on joint diseases were assessed by body weight, arthritis index (AI) score, swollen joint count (SJC) score, and hind paw thickness. Ankle radiological changes were captured by micro-computed tomography (micro-CT) and histological changes were observed by pathological staining. Organ histological changes, spleen index, alanine aminotransferase (ALT), aspartate aminotransferase (AST), and creatinine (Crea) levels of serum were tested to evaluate the toxicity of MAI. Cytokine expression levels were confirmed by enzyme-linked immunosorbent assay (ELISA) to evaluate the immunity of CIA mice.

Results: MAI administration markedly improved the clinical signs of CIA in mice, including hind paw thickness, AI, and the number of swollen paw joints (most of them $P<0.05$ or even <0.01). According to histopathological analysis, MAI ameliorated inflammatory cell infiltration, synovial hyperplasia, pannus formation, and bone erosion (all $P<0.01$). Micro-CT and tartrate-resistant acid phosphatase (TRAP) staining ($P<0.01$) also revealed that MAI could relieve bone erosion via reducing the formation of osteoclasts. Not only could MAI relieve the immunological boost [$P<0.05$ for the high-dose MAI (HM) group], but also it had no liver or kidney side effects ($P>0.05$). In addition, it decreased the serum levels of interleukin (IL)-6 and tumor necrosis factor-α (TNF-α) and increased the serum levels of IL-4 and IL-10 (the majority of $P<0.05$

or even <0.01). Transcriptome sequencing results indicated that MAI affected the expression of osteoclast differentiation pathway genes, which was connected with the receptor activator of the nuclear factor κB ligand/nuclear factor kappa B (RANKL/NF-κB) pathway.

Conclusions: Based on our findings, MAI could suppress joint inflammation and inhibit RANKL/NF-κB-mediated osteoclast differentiation to rescue bone erosion in CIA mice, suggesting that MAI can be a potentially therapeutic substance for RA.

Keywords: Melittin acupoint injection; collagen-induced arthritis; bone erosion; receptor activator of the nuclear factor κB ligand/nuclear factor kappa B (RANKL/NF-κB) signaling pathway

Submitted Mar 01, 2023. Accepted for publication Jul 06, 2023. Published online Jul 20, 2023.
doi: 10.21037/qims-23-254
View this article at: https://dx.doi.org/10.21037/qims-23-254

Introduction

Rheumatoid arthritis (RA) is a chronic autoimmune disease with unclear etiology, characterized by synovial inflammation, pannus formation, articular cartilage destruction, and bone erosion (1). According to an epidemiological survey, approximately 1% of the world's population has RA, with a female preponderance (2). A study showed that the global age-standardized prevalence of RA increased by 7.4% and the incidence by 8.2% between 1990 and 2017. During this period, the number of years living with disability globally attributable to RA as a percentage of the worldwide total years with disability increased from 0.24 % to 0.31% (3).

Currently, the main anti-RA therapeutics include antirheumatic drugs, nonsteroidal anti-inflammatory drugs, glucocorticoids, and biological agents. As a result of occasionally serious side effects (4,5), the effectiveness of these drugs is far from satisfactory and cannot meet the demand of all patients with RA. Bone erosion is the cause of disability in RA; it usually appears early in the development of RA and accompanies the entire progression of the disease, which is closely related to innate immune mechanisms, autoimmunity, and synovitis (6,7). RA bone erosion is rarely repaired, and spontaneous repair is almost nonexistent (6). Consequently, there is an urgent need to identify effective treatment methods and avoid the further development of RA in its early treatment.

Melittin, which accounts for 40–60% of the whole dry venom (8), is originally separated and purified from honey bee (*Apis mellifera*) venom and is the main active ingredient (8,9). Melittin has various biological, pharmacological, and toxicological properties, including those conferring anti-arthritic, anti-tumor, anti-infection, and neuroprotective effects, among others (10-13). Melittin mainly plays an anti-arthritic and pain-relieving role in RA, and delays the progression of RA disease, thus alleviating the bone erosion of RA. A study (10) reported that polymeric microneedle-mediated transdermal delivery of melittin could effectively suppress RA progression in adjuvant-induced arthritis, as indicated by the reduction in paw swelling and arthritis score, inhibition of interleukin (IL)-17 and tumor necrosis factor-α (TNF-α), and increased percentage of regulatory cluster of differentiation 4 (CD4) T cells.

It is well known that traditional Chinese medicine (TCM) is widely used in RA, including decoction, acupuncture, moxibustion, and acupoint injection methods. A study showed that the Chinese herbal medical formula Fufang Shatai Heji exerts a cartilage protective effect by inhibiting the expression of matrix metalloproteinases (MMPs) in collagen-induced arthritis (CIA) mice (14). Acupoint injection is a treatment in which drugs are injected into specific acupoints, such as Zusanli (ST36), to stimulate these points and thus achieve therapeutic effects (15). It is an alternative supplementary therapy based on the meridian theory, which belongs to the category of TCM. Acupoint injection has the dual function of drug delivery and acupuncture, so it is more effective than Western medicine alone (16). It is currently used in a variety of diseases, such as type 2 diabetic peripheral neuropathy, stroke accompanied by hemiplegia, and arthritis (16-18).

Both melittin and acupoint injection are closely related to the treatment of RA. Melittin acupoint injection (MAI) has the effects of melittin drug administration and acupuncture. The receptor activator of the nuclear factor κB ligand/nuclear factor kappa B (RANKL/NF-κB) pathway is one of the pathways involved in osteoclast differentiation, and

blocking this pathway has been shown to reduce bone erosion in CIA mice (19). However, the pharmacological mechanism of MAI in treating RA is still unclear, and whether its effect on RA bone erosion is via the RANKL/NF-κB pathway has not been evaluated. Therefore, this study aimed to investigate the regulatory effect of MAI on joint bone erosion in CIA mice and to elucidate the underlying mechanism. We present this article in accordance with the ARRIVE reporting checklist (available at https://qims.amegroups.com/article/view/10.21037/qims-23-254/rc).

Methods

Animals

A total of 48 7–8-week-old male DBA/1 mice weighing 18–20 g were obtained from Charles River Laboratories (Beijing, China) and then housed in a specific-pathogen-free (SPF) level laboratory under standard conditions (25±1 ℃, 12-h light-dark cycle, and 60%±10% humidity) with free access to water and food. Before the experiment, they had to adapt to the environmental conditions for 1 week. Animal experiments were performed under a project license (No. SMUL2022024) granted by the Ethics Committee of Southern Medical University, in compliance with Southern Medical University guidelines for the care and use of animals. A protocol was prepared before the study without registration.

Materials and reagents

Melittin was purchased from Shanghai Aladdin Biochemical Technology (Shanghai, China). Bovine type II collagen solution [20022], complete Freund's adjuvant [7009], and incomplete Freund's adjuvant [7002] were acquired from Chondrex (Woodinville, WA, USA). A hematoxylin and eosin (HE) staining kit, a safranin O-fast green (SafO) staining kit, and a tartrate-resistant acid phosphatase (TRAP) staining kit were obtained from Solarbio (Beijing, China); IL-4, IL-6, IL-10, and TNF-α, enzyme-linked immunosorbent assay (ELISA) kits were procured from Mlbio (Shanghai, China); aspartate aminotransferase (AST), alanine aminotransferase (ALT), and creatine (Crea) kits were provided by Nanjing Jiancheng Bioengineering Institute (Nanjing, China); 10% ethylene diamine tetraacetic acid (EDTA) decalcified fluid was purchased from Leagene Biotechnology (Beijing, China).

Establishment of the CIA model and treatment

The CIA animal model was established as previously described (20). Briefly, on day 0, 40 randomly selected male mice were injected intradermally with a mixture of 100 μL of emulsion containing 100 μg of bovine type II collagen solution (2 mg/mL) and an equal volume of complete Freund's adjuvant (2 mg/mL) at the base of the tail as the first immunization.

On day 21, the mice were given a booster immunization with 100 μg of bovine type II collagen solution emulsified in equal volumes of incomplete Freund's adjuvant by the same route. The normal control group mice (NC; n=8) were injected in the same way with saline. Mice were then monitored daily for arthritis progression. Special care was taken to ensure that all mice had adequate access to food and water during the development of the disease.

On day 28, CIA mice were randomly assigned into 5 groups: a CIA model group (MO; n=8), a methotrexate group (MT; n=8), a low-dose MAI group (LM; n=8), a medium-dose MAI group (MM; n=8), and a high-dose MAI group (HM; n=8). The acupoint ST36 was located near the knee joint of the hind limbs, 1.5 mm distal to the distal anterior tibial tubercle (21). Except for those in the MT group, all mice received MAI once every other day beginning from the 28th day of the experiment. For the LM, MM, and HM groups, ST36 was positioned, and 0.25, 0.5, and 1.0 mg/kg of melittin was injected, respectively (16). A melittin solution (0.02 mL) was administered at ST36 on both sides in turn each time. The NC and MO group were administered an equal volume of saline. The MT group was given a dose of 2 mg/kg of methotrexate (MTX) once a week intragastrically. All the mice were treated for 28 days and were euthanized under anesthesia. Blood, joint tissues, and internal organs were harvested for further study.

Assessment of arthritis

Beginning on day 28 after the initial immunization, arthritis index (AI) score, swollen joint count (SJC) score, hind paw thickness, and body weight were evaluated every 4 days. AI scores were measured from 0 to 4 points for each limb under the following scoring system: 0 point, normal, no redness or swelling; 1 point, swelling and/or redness of the interphalangeal joints; 2 points, involvement of 3 to 4 interphalangeal joints or 1 larger joint; 3 points, severe redness and swelling of the paw below the ankle; and

4 points, severe arthritis of an entire paw including the ankle (22,23). The values for the 4 paws contributed to the total score, and the highest was 16 points. The SJC score was evaluated as previously reported: the ankle (or wrist) and 5 finger (toe) joints of each limb were calculated, with the highest possible score being 24 points (23). Moreover, the thickness of the hind paws was measured with vernier calipers. Scoring and hind paw thickness measurements were carried out by 2 researchers blinded to the treatment group of the animal. Additionally, the changes in the body weight of each mouse were calculated.

Spleen index measurement

Mice were euthanized on day 56 after the initial immunization. The spleens were collected, washed in 4 ℃ phosphate-buffered saline (PBS) solution, blotted with filter paper, and weighed. The spleen index was calculated as follows: spleen index (‰) = spleen mass (g)/body weight (g) × 1,000 (24).

Micro-computed tomography analysis

After euthanasia of the mice, the right ankle joints were immediately dissected and fixed in 4% paraformaldehyde at 4 ℃ for 1 week. To evaluate bone focal erosion in the ankle joint, 3-dimensional (3D) reconstructions were obtained by micro-computed tomography (micro-CT; ZKKS-MCT-Sharp, Zhongke Kaisheng Medical Technology, Guangzhou, China) with the following parameters: scanning voltage, 70 kv; power, 7 w; angle gain, 0.72°; exposure time, 100 ms; and number of superimposed frames, 4. The scanning was completed after 1 rotation. The scanned images were observed and analyzed using a 3D medical image processing and analyzing system (3Dmed v. 5.2 software; Key Laboratory of Molecular Imaging, Chinese Academy of Sciences, Beijing, China).

HE staining and analysis

After micro-CT scanning, the ankle joints were decalcified in 10% EDTA solution and embedded in paraffin. The spleen, liver, and kidney were fixed directly for 1 week in 4% paraformaldehyde. Sections (5 μm) were stained with HE, SafO, or TRAP.

The degree of right ankle histopathological damage was based on previously described criteria and scored on a scale of 0–3 according to the degree of synovitis, pannus, and destruction of cartilage and bone, as follows (25): grade 0, normal; grade 1, mild synovitis with hyperplastic membrane and no inflammatory reaction; grade 2, moderate synovitis, no pannus formation, and localized bone and cartilage destruction; and grade 3, severe synovitis with pannus formation, extensive bone and cartilage erosions, and disordered joint architecture. Histopathological analysis was evaluated by independent observers in a blinded manner.

SafO staining and analysis

The paraffin sections of right ankle tissue were prepared for staining with SafO. The combination of basophil cartilage and basic dye saffron O shows red, whereas the combination of eosinophilic bone and the acid dye fast green shows green or blue, which is in sharp contrast with red cartilage, which can distinguish between cartilage and bone tissue. The cartilage erosion in arthritic joints was scored on a scale of 0–3 as described previously (26). Similarly, scoring was performed by 2 investigators with blinding, and the mean of both scores was calculated.

TRAP staining and analysis

The paraffin section of right ankle tissue was prepared for TRAP staining to identify osteoclasts. All steps were performed in strict accordance with the relevant kit instructions. If purplish red granulation appeared on the tissue, it was considered a positive reaction. TRAP-positive cells were captured using a pathological section scanner (KFBIO, Yuyao, China) on the slides (magnification 100×), and the expression rate of positive cells was quantified using ImageJ software (National Institutes of Health, Bethesda, MD, USA).

Serum cytokines assay and biochemical measurement

Blood was collected from mice at the end of the experiment. After centrifugation at 3,500 rpm for 15 minutes at 4 ℃, the serum was collected, and the levels of IL-4, IL-6, IL-10, and TNF-α were assessed with ELISA kits according to the manufacturer's protocols. Hepatotoxicity was determined by measuring serum levels of AST and ALT, and renal toxicity assessed by measuring serum Crea.

Transcriptome sequencing and bioinformatics analysis

Left ankle tissues were selected from the NC, MO,

and MM groups (n=3 each group) for studies. Library construction, messenger RNA sequencing (mRNA-seq), and bioinformatic analysis were commissioned to Majorbio Bio-pharm Technology (Shanghai, China). The general workflow was as follows: RNA extraction and detection; mRNA enrichment, fragmentation, and reverse transcription into complementary DNA (cDNA); cDNA end repair, a-tailing, and sequencing adapters; and polymerase chain reaction (PCR) enrichment and library construction. An Illumina NovaSeq 6000 (Illumina, San Diego, CA, USA) was used for RNA sequencing.

Sample quality was assessed first, and the samples were qualified only when they met the following quality control requirements: the average error rate (%) of sequencing bases was less than 0.1%, and quality score 20 (Q20) was above 85% whereas the quality score 30 (Q30) was above 80% in the sample. Then, cluster analysis was performed to evaluate gene expression correlation. Taking $P<0.05$ and fold change =1.8 as the threshold for significant differential expression, differential genes or transcripts were screened for Gene Ontology (GO) annotations analysis and Kyoto Encyclopedia of Genes and Genomes (KEGG) pathway enrichment analysis. Ultimately, target genes were selected from the differential genes for protein network interaction analysis (https://cn.string-db.org/).

Statistical analyses

All quantitative data were presented as the mean ± standard deviation (SD) of 3 independent experiments. Statistical analyses were performed with the software SPSS 22.0 (IBM Corp., Armonk, NY, USA). One-way analysis of variance (ANOVA) was used to evaluate the statistical significance of differences in multigroup-designed experiments, which was followed by the least significant difference (LSD) post hoc analyses for multiple groups. A P value <0.05 was considered statistically significant.

Results

MAI ameliorated arthritis in CIA mice

To evaluate the therapeutic effect of MAI on the CIA model, a classic RA animal model was established by injecting complete Freund's adjuvant or incomplete Freund's adjuvant simulated bovine type II collagen solution, and MAI was administrated 28 days later (*Figure 1A*). After 4 weeks of treatment, the effects of MAI on arthritis were analyzed. As illustrated in *Figure 1B*, the forepaw and hind paw arthritis of the treatment group was relieved after treatment. The body weights of the MO group significantly decreased to different degrees compared to the NC group throughout the experiment. However, none of the treatment groups showed significant difference in body weight compared to the MO group during the experimental period (*Figure 1C*). Interestingly, the MO group displayed consistently and significantly increased AI scores and SJC scores. On the contrary, the administration of MAI or MTX significantly reduced AI and SJC scores in arthritis mice (*Figure 1D,1E*).

Additionally, the hind paw thickness of CIA mice gradually increased on days 28–36, and then gradually decreased after reaching their peak on day 36. The hind paw thickness in the MO group was significantly higher than that in the NC group during the treatment period. Nevertheless, MAI treatment improved these symptoms in the therapeutic groups compared with the MO group. Moreover, similar to MAI, the approved drug MTX exerted similar effects on suppressing the development of hind paw thickness (*Figure 1F*), which indicated that both MAI and MTX demonstrated significant amelioration on joint swelling and inflammation. Therefore, our data demonstrated that MAI ameliorated arthritis in mice, suggesting the protective role of MAI in arthritis.

Safety of MAI in CIA mice

Considering the safety of MAI in biological and clinical applications, we measured spleen index, HE staining, and hematological parameters in mice injected with various dosages of melittin. It is well known that the relative organ weights of the spleen and HE staining are important indicators of immunological function. The pathological staining and biochemical measurement of the liver and kidneys could indicate the hepatorenal toxicity of the therapeutic agents applied to the mice.

As shown in *Figure 2A,2B*, the spleen volume and organ index were significantly increased in the MO group compared to the NC group. After drug administration, the spleen index decreased compared with the MO group. There were significant differences in the relative weights of the spleen between the MO and HM groups. Meanwhile, HE staining of the spleen revealed significant white and red pulp hyperplasia, and germinal center appearance of all the MO group mice. In contrast, MAI- and MTX-treated mice exhibited only slight pathological changes (*Figure 2C*). In

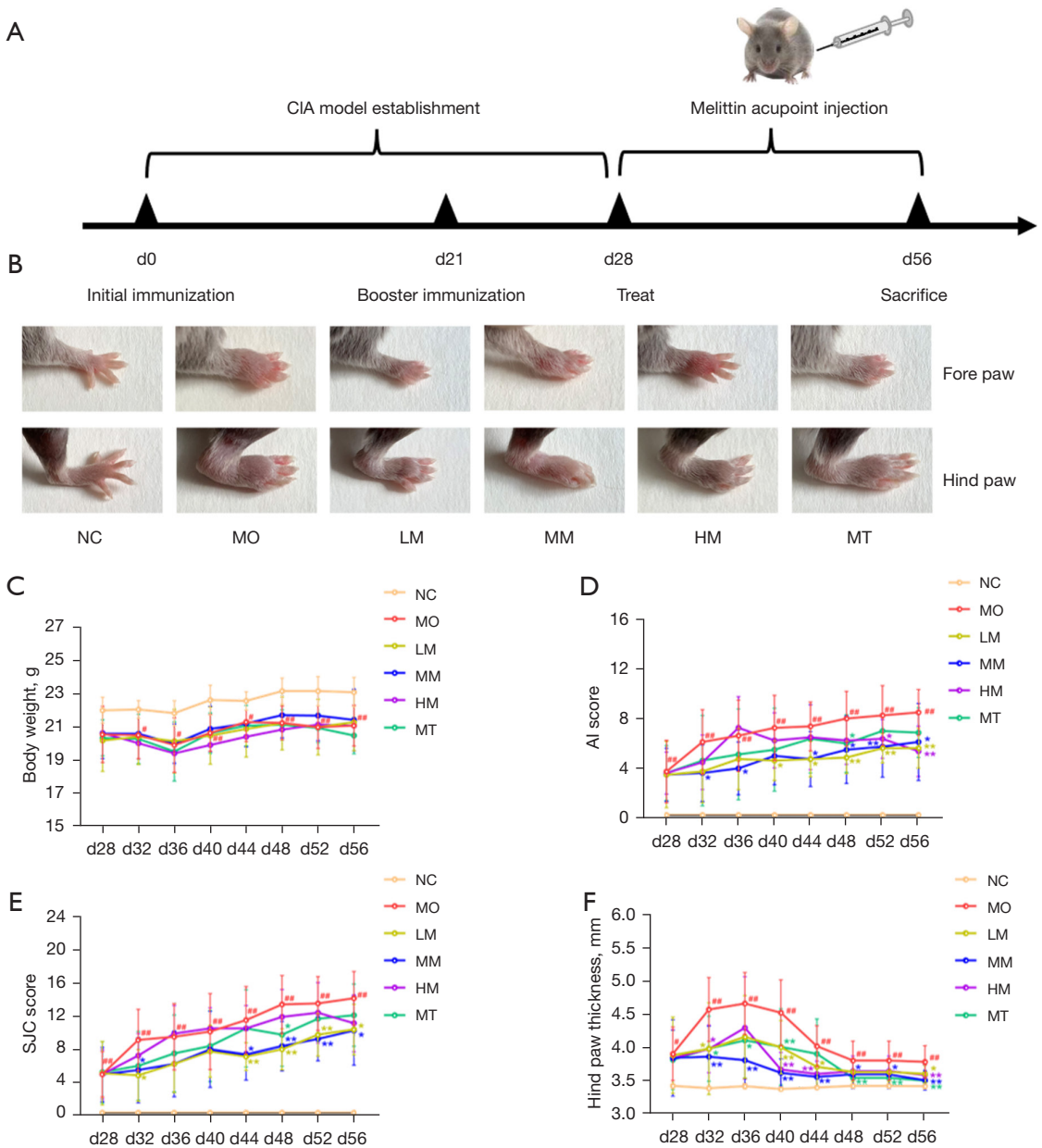

Figure 1 Effect of MAI on the symptoms in CIA mice. (A) Experimental design. Mice were treated on day 28 after primary immunization. (B) Photographs of representative paws from mice after finishing treatment. (C) Body weight. (D) AI score. (E) SJC score. (F) Hind paw thickness. All data are presented as the mean ± SD (n=8). $^{\#}$, P<0.05 or $^{\#\#}$, P<0.01 *vs.* NC group, *, P<0.05 or **, P<0.01 *vs.* MO group. CIA, collagen-induced arthritis; NC, normal control group; MO, CIA model group; LM, low-dose MAI group; MM, medium-dose MAI group; HM, high-dose MAI group; MT, methotrexate group; AI, arthritis index; SJC, swollen joint count; MAI, melittin acupoint injection; SD, standard deviation.

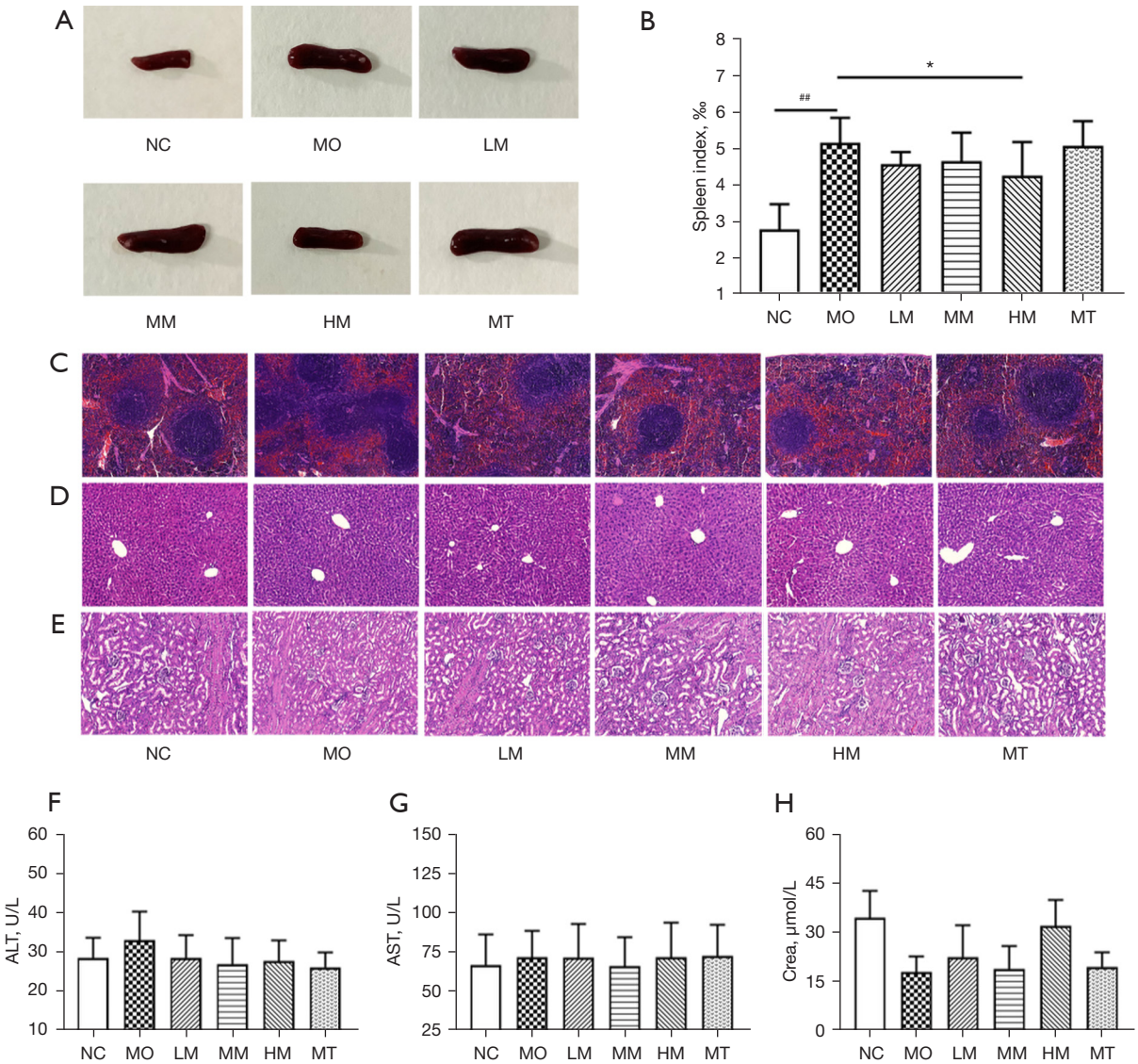

Figure 2 Effect of MAI on the visceral organ toxicity in CIA mice. (A) Gross view of splenic tissue at the time the mice were killed. (B) Spleen index. (C-E) Spleen, liver, and kidney HE staining (magnification, ×100). (F,G) ALT and AST in mice serum. (H) Crea in mice serum. Results are shown as the mean ± SD (n=8). ##, P<0.01 *vs.* NC group, *, P<0.05 *vs.* MO group. NC, normal control group; MO, CIA model group; LM, low-dose MAI group; MM, medium-dose MAI group; HM, high-dose MAI group; MT, methotrexate group; ALT, alanine transaminase; AST, aspartate aminotransferase; Crea, creatine; MAI, melittin acupoint injection; CIA, collagen-induced arthritis; HE, hematoxylin and eosin; SD, standard deviation.

addition, the pathological examination of liver and kidney interestingly showed that MAI had no toxic effect on the liver and kidney (*Figure 2D,2E*). Furthermore, the ALT, AST, and Crea levels fell within the normal range (P>0.05; *Figure 2F-2H*).

Collectively, our data suggested that MAI could alleviate the immunological boost due to the induction of CIA without inducing liver or kidney side effects.

MAI inhibited bone erosion in CIA mice

Micro-CT and histologic scores were used to estimate the influence of MAI on bone destruction in CIA mice. High-resolution scanning images using micro-CT

(*Figure 3A*) revealed the curative effect of MAI on bone and joint destruction. Compared with the NC group, the MO group had severe bone surface roughness, bone resorption, and decreased bone density with narrow joint space. Meanwhile, MAI and MTX treatment attenuated joint destruction, especially in the MM group.

The pathological changes of the joint tissues were observed under the microscope and scored (*Figure 3B,3C*). HE staining showed that there were obvious inflammatory cell infiltration, pannus formation, cartilage erosion, or bone destruction in the MO group. The histopathology and necrosis were so extensive that it was difficult to identify the intact articular cavity. In contrast with the MO group, MAI and MTX effectively reduced these histological severity scores.

Similar results were obtained by analyzing ankle joint sections stained with SafO (*Figure 3D,3E*). Substantial proteoglycan loss and cartilage erosion were observed in CIA mice treated with saline, suggesting severe degradation and destruction of articular cartilage tissue. Cartilage was less damaged in animals treated with MAI and MTX.

TRAP, as a specific marker enzyme of osteoclasts, was specifically distributed in the cytoplasm of osteoclasts. If the cells showed tartaric acid resistance, the cytoplasm of the cells was purple or purplish-red (positive granules) after TRAP staining solution was added. Accordingly, the functional status of osteoclasts could be understood by observing the positive particles in the sections. Abundant osteoclasts in the ankle joints of the MO group mice were characterized by TRAP staining. In contrast with the MO group, MAI and MTX administration significantly reduced the number of osteoclasts in the treatment group, as shown in *Figure 3F,3G*. In general, these findings indicated that MAI prevented bone erosion to a certain extent.

MAI decreased serum levels of proinflammatory cytokines and increased serum levels of anti-inflammatory cytokines in CIA mice

Multiple proinflammatory cytokines, including IL-6 and TNF-α, not only induced and exacerbated inflammation but also caused cartilage damage and bone destruction in RA, whereas IL-4 and IL-10 had the opposite effect. The imbalance between pro- and anti-inflammatory cytokines activities is well acknowledged to favor the induction of autoimmunity in RA (27,28). Hence, we investigated whether MAI exerted regulatory effects on the functions of pro- and anti-inflammatory cytokines.

As can be seen in *Figure 4A,4B*, the serum levels of IL-6 and TNF-α in the MO group mice were increased, whereas MAI and MTX administration could significantly decrease the levels of the above 2 cytokines. Compared with that in the NC group, the levels of serum IL-4 and IL-10 in the MO group were significantly decreased ($P<0.01$). Meanwhile, the increase of serum IL-10 level in HM ($P<0.01$) and MT ($P<0.05$) groups were statistically significant compared to the MO group. Nonetheless, 3 different doses of MAI and positive drugs could increase IL-4 and IL-10 levels (*Figure 4C,4D*). These findings suggested that MAI could regulate the secretions of both proinflammatory and anti-inflammatory cytokines in CIA models.

MAI affected the expression of osteoclast differentiation pathway genes

According to the above research results, the MM group was selected as the representative to conduct ankle mRNA-seq study with the NC and MO groups. The 3 groups of samples were extracted and sequenced for mRNA. On the whole, the quality inspection results of the samples in this study all met the quality control requirements, indicating that the test results and data analysis were credible (*Table 1*).

To analyze the expression patterns and expression levels of different genes/transcripts, cluster analysis was performed in this study. In cluster analysis, the closer the expression pattern of all genes/transcripts in 2 samples is, the closer the trend of their expression quantity. According to the heat map figures (*Figure 5A*), the expression patterns of the NC and MM group were close to each other, whereas the MO group was opposite to NC and MM group. These results indicated that MAI treatment was effective, because the gene expression of the MM group mice after therapy gradually tended to be closer to the NC group, whereas the MO group did not show this change.

Subsequently, the genes/transcripts detected were screened for statistically significant differences under the conditions of $P<0.05$ and fold change =1.8 as the threshold. Compared with the NC group, a total of 4,550 differentially expressed genes (DEGs) were screened in the MO group, including 2,268 upregulated genes and 2,282 downregulated genes. After the intervention of MAI, 891 upregulated genes and 813 downregulated genes were found in the MM group compared to the MO group (*Figure 5B*).

Sequentially, we further analyzed the DEGs. As can be seen from *Figure 5C*, GO annotation distribution included

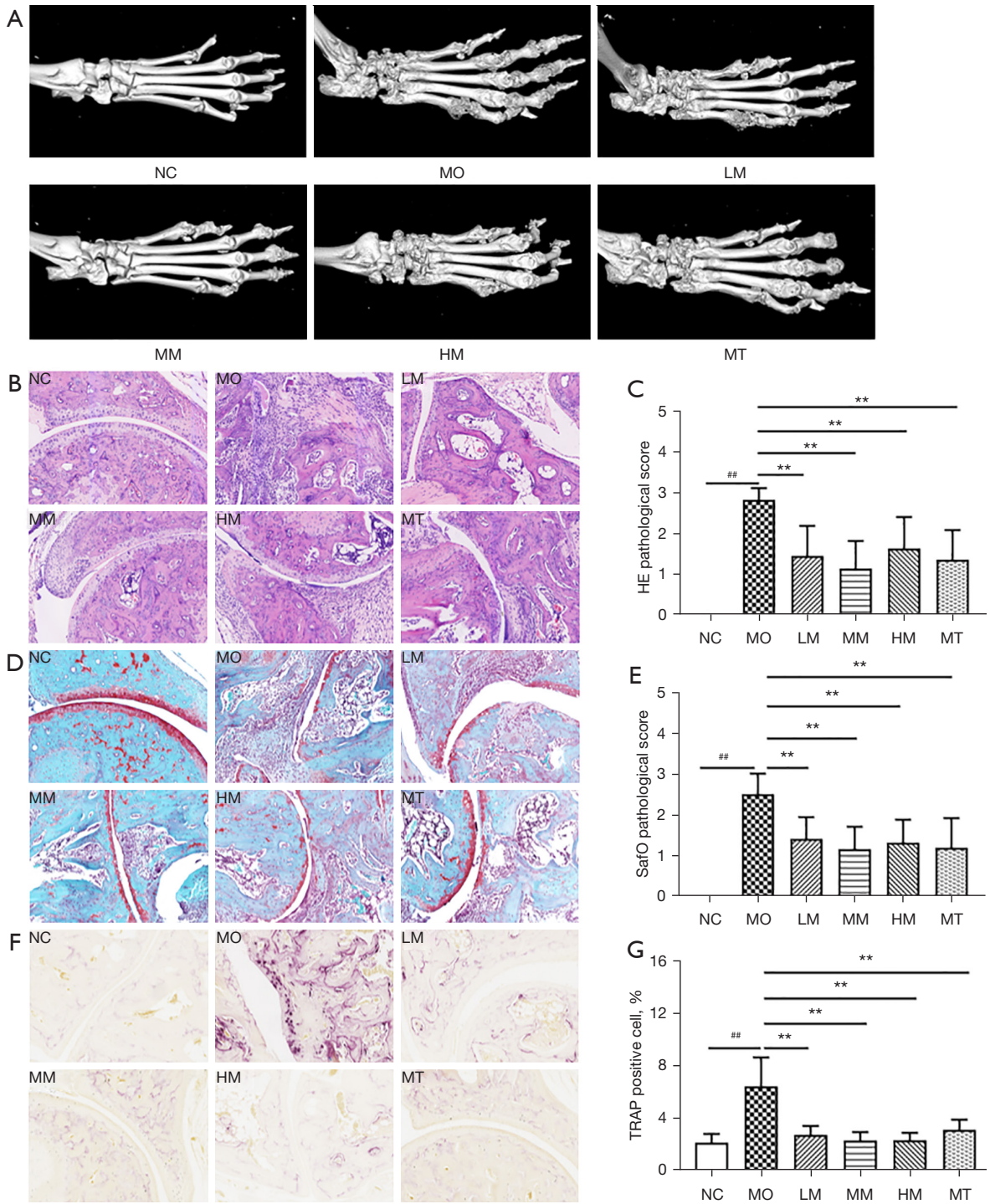

Figure 3 Effect of MAI on joint pathology in CIA mice. (A) Representative micro-CT 3-dimensional images of the ankle joint (n=3). (B,C) Ankle joint HE staining (magnification, ×100) and histopathological inflammatory scores. (D,E) Ankle joint SafO staining (magnification, ×100) and histopathological inflammatory scores. (F,G) Ankle joint TRAP staining (magnification, ×100) and TRAP-positive osteoclast percentage. Results in parts (B-G) are shown as the mean ± SD (n=8). ##, P<0.01 *vs.* NC group; **, P<0.01 *vs.* MO group. NC, normal control group; MO, CIA model group; LM, low-dose MAI group; MM, medium-dose MAI group; HM, high-dose MAI group; MT, methotrexate group; HE, hematoxylin and eosin; SafO, safranin O-fast green; TRAP, tartrate-resistant acid phosphatase; MAI, melittin acupoint injection; CIA, collagen-induced arthritis; CT, computed tomography.

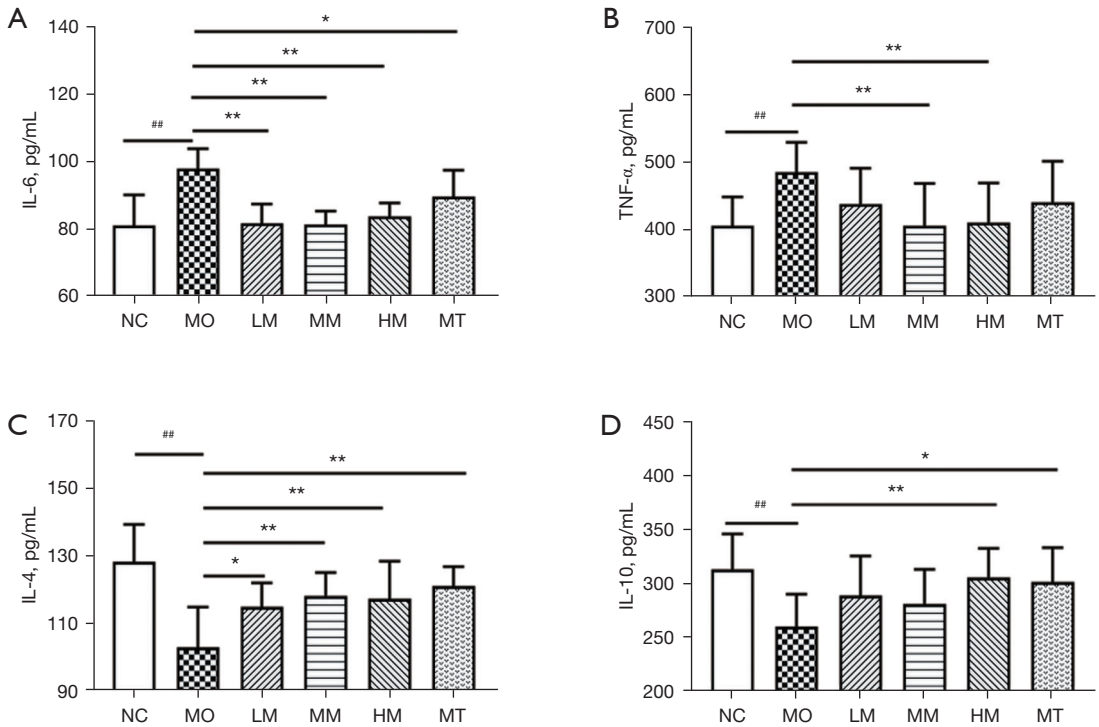

Figure 4 Effect of MAI on the expression of inflammatory cytokines. (A) IL-6, (B) TNF-α, (C) IL-4, and (D) IL-10 in mice serum after treatment. Data are represented as the mean ± SD (n=8). ##, P<0.01 *vs.* NC group; *, P<0.05 or **, P<0.01 *vs.* MO group. NC, normal control group; MO, CIA model group; LM, low-dose MAI group; MM, medium-dose MAI group; HM, high-dose MAI group; MT, methotrexate group; IL, interleukin; TNF, tumor necrosis factor; MAI, melittin acupoint injection; SD, standard deviation; CIA, collagen-induced arthritis.

3 parts: biological process (BP), cellular component (CC), and molecular function (MF). From the perspective of BP, biological regulation and cellular processes were more involved. Cells and organelles were significantly enriched in CC, and blinding also had a strong significance in MF. The bubble plot in *Figure 5D* shows the top 20 pathways enriched by KEGG. These pathways included osteoclast differentiation, RA, cytokine-cytokine receptor interaction, the NF-κB signaling pathway, TNF signaling pathway, IL-17 signaling pathway, and calcium signaling pathway, among others, which were all related to autoimmunity and inflammation. As the osteoclast differentiation pathway was of particular interest to our research, a total of 32 DEGs (i.e., target genes) in the osteoclast differentiation pathway were screened out, including 28 downregulated genes and 4 upregulated genes, as shown in *Table 2*.

Ultimately, 32 target genes were uploaded to the STRING (Search Tool for the Retrieval of Interacting Genes/Proteins) database to analyze protein interactions. It could be seen that the *Gpc3* and *Map2k6* genes were not found to interact with each other. Among the other 30 genes, *Tnfsf11* (RANKL), *Nfkb2*, *Relb*, *Fos*, *Junb*, *Acp5* (TRAP), *Ctsk*, *Oscar*, *Ocstamp*, *Atp6v0d2*, and others, had a wide range of interactions (*Figure 6*). This study found that MAI affected the genes of osteoclast differentiation pathway, with the RANKL/NF-κB pathway being the most closely related to osteoclast differentiation. Consequently, we found that MAI could inhibit bone destruction in CIA mice, likely via inhibiting osteoclast differentiation mediated by the RANKL/NF-κB pathway.

Discussion

In this study, we focused on the effect of MAI treatment on a CIA mouse model. As previously described (29), the CIA mice showed weight loss, severe arthritis, joint swelling, and pathological change of inflammatory cell infiltration, pannus formation, and joint destruction. These

Table 1 Assessment of transcriptome sample quality

Sample	Raw reads	Raw bases	Clean reads	Clean bases	Error rate (%)	Q20 (%)	Q30 (%)	GC content (%)
NC_1	50838896.00	7676673296.00	48723532.00	7179869674.00	0.03	97.42	92.89	50.03
NC_2	43597456.00	6583215856.00	41613634.00	6104604978.00	0.03	97.01	91.86	50.01
NC_3	46249712.00	6983706512.00	44392506.00	6543592130.00	0.03	97.33	92.67	49.97
MO_1	51578442.00	7788344742.00	50265860.00	7310689606.00	0.03	97.21	92.31	51.49
MO_2	45027350.00	6799129850.00	43999112.00	6404791918.00	0.03	97.44	92.77	51.57
MO_3	43920450.00	6631987950.00	42360782.00	6194500928.00	0.03	97.01	91.93	49.23
MM_1	49729902.00	7509215202.00	48057796.00	7004714137.00	0.03	97.32	92.56	50.27
MM_2	48480050.00	7320487550.00	46879718.00	6858385049.00	0.03	97.38	92.73	50.62
MM_3	46988918.00	7095326618.00	45618064.00	6671715606.00	0.03	97.23	92.38	50.92

NC, normal control group; MO, CIA model group; MM, medium-dose MAI group; Q20, quality score 20; Q30, quality score 30; GC, guanine and cytosine; CIA, collagen-induced arthritis; MAI, melittin acupoint injection.

manifestations demonstrated that the model establishment met the experimental criteria. From these outcomes, it was easy to conclude that MAI can improve clinical symptoms and pathological lesions without liver or kidney damage. Surprisingly, bone erosion was rescued after the MAI administration. Moreover, MAI decreased proinflammatory cytokines levels and increased anti-inflammatory cytokines in CIA mice, which suggested that MAI could not only reduce the infiltration of joint inflammatory cells, but also regulated the levels of proinflammatory and anti-inflammatory factors in serum. Likewise, the results indicated that MAI could affect osteoclast differentiation by suppressing the RANKL/NF-κB signaling pathway. This was the first time that MAI was applied to CIA mice, and the experimental results showed that MAI had strong anti-arthritic and osteoprotective effects. Bee venom is produced by female worker bees and contains many active components, including melittin, apamin, mast cell degranulating peptide, phospholipase A2, hyaluronidase, amino acids, and other compounds (9). As mentioned above, melittin, as the main component responsible for the pharmacological effect, is widely used in clinical practice, especially in RA. However, bee venom often leads to allergic reactions, with phospholipase A2 being the main allergen (30). Recently, a study (31) found that the detoxification of bee venom (with melittin as its retained active component) could not only increase its anti-inflammatory activity but also decrease its cytotoxic and allergic activity. In other words, melittin can both play an anti-inflammatory role and reduce allergic reactions. This is why melittin was chosen for acupoint injection in this study.

ST36 is an acupoint on the stomach meridian of the Foot-Yangming channel in TCM, with the functions of dispelling pathogenic wind and removing dampness, relieving rigidity of muscles, and activating collaterals. It can thus confer anti-inflammatory and analgesic effects and is a commonly used acupoint for treating RA. It was previously found that ST36 acupuncture could alleviate paw edema, upregulate the nociceptive threshold, and inhibit immune cell communication networks to improve adjuvant-induced arthritic symptoms. Equally, manual acupuncture at ST36 has also been shown to ameliorate RA by suppressing M1 macrophage polarization and elevating regulator T cell (Treg) populations in adjuvant-induced arthritis rats (32,33). Our experimental results were consistent with these findings, which once again confirmed that MAI has a good effect on RA.

According to osteoimmunology, the immune system and the skeletal system share a variety of cytokines, chemokines, transcription factors, and signaling molecules, and they interact and regulate bone formation and resorption (34). It is well known that under physiological conditions, bone remodeling continues to occur as a coordinated process leading to bone formation and degradation, which maintains a balance between osteoblast-mediated bone formation and osteoclast-regulated bone absorption, thus ensuring bone homeostasis. Under pathological conditions, excessive activation of osteoclasts results in abnormal bone resorption and destruction of bone homeostasis, leading to abnormal osteoclast formation (7,35). Many studies maintain that

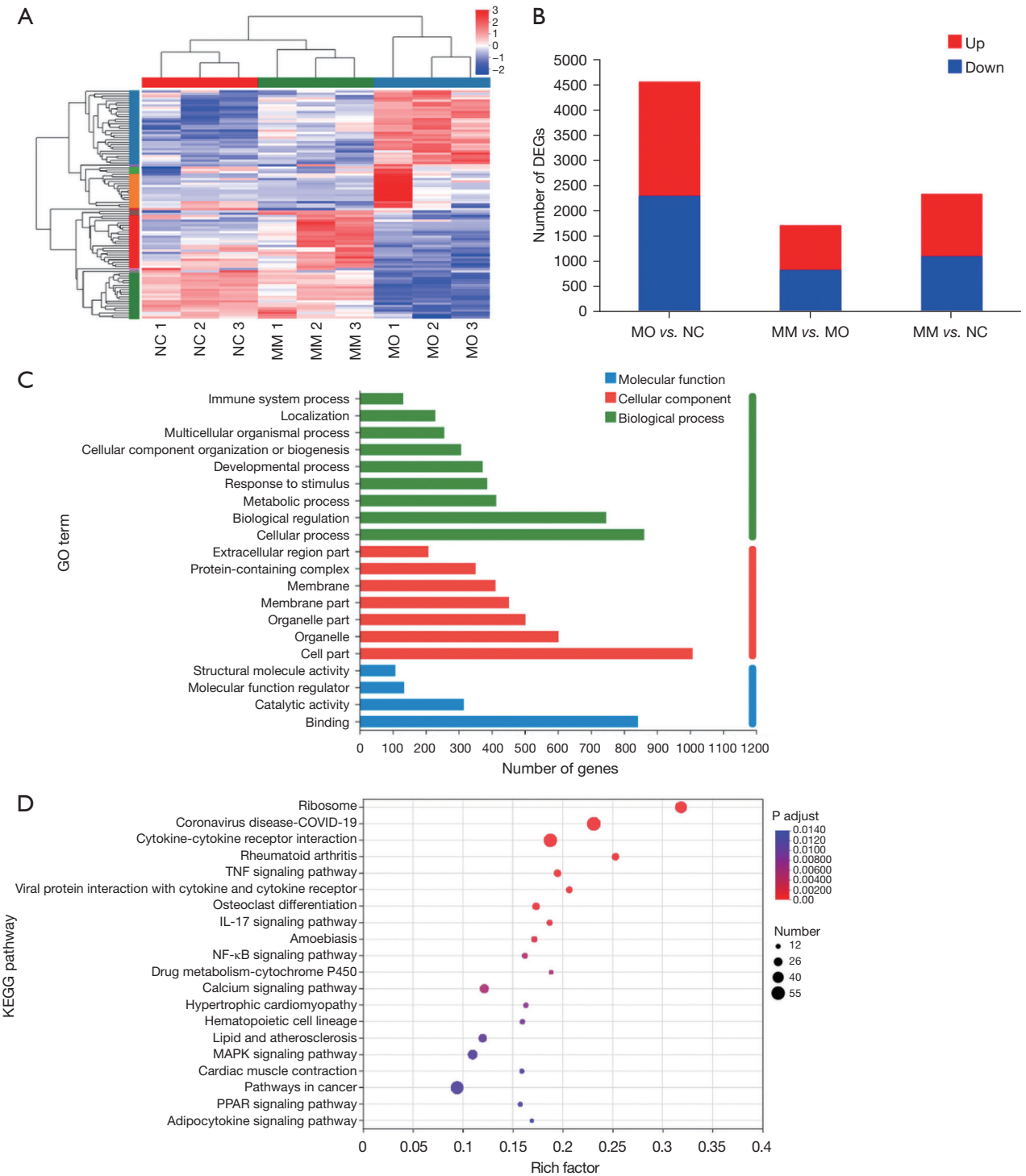

Figure 5 Effect of MAI on the inhibition of osteoclast differentiation in CIA mice (n=3). (A) Heatmap. (B) Differential gene statistic. (C) GO annotations analysis. (D) Top 20 KEGG pathway enrichment analysis. DEGs, differentially expressed genes; MO, CIA model group; NC, normal control group; MM, medium-dose MAI group; GO, Gene Ontology; KEGG, Kyoto Encyclopedia of Genes and Genomes; TNF, tumor necrosis factor; IL, interleukin; NF, nuclear factor; MAI, melittin acupoint injection; CIA, collagen-induced arthritis; SD, standard deviation.

Table 2 The differential genes related to osteoclast differentiation in this study

Gene name	Gene description	FC (MM/MO)	Log2FC (MM/MO)	P value	Regulation
Il1b	Interleukin 1 beta	0.134292	−2.8965497	0.0000	Down
Fosl1	Fos-like antigen 1	0.154761	−2.6918851	0.0000	Down
Socs3	Suppressor of cytokine signaling 3	0.295596	−1.7583011	0.0000	Down
Fosb	FBJ osteosarcoma oncogene B	0.296927	−1.7518192	0.0012	Down
Sirpb1b	Signal-regulatory protein beta 1B	0.301659	−1.7290115	0.0000	Down
Tnfsf11	Tumor necrosis factor (ligand) superfamily, member 11	0.340598	−1.5538601	0.0000	Down
Oscar	Osteoclast associated receptor	0.359699	−1.4751398	0.0076	Down
Ocstamp	Osteoclast stimulatory transmembrane protein	0.382262	−1.3873659	0.0035	Down
Sirpb1c	Signal-regulatory protein beta 1C	0.404903	−1.3043517	0.0000	Down
Tyrobp	TYRO protein tyrosine kinase binding protein	0.418965	−1.2550995	0.0000	Down
Junb	Jun B proto-oncogene	0.436807	−1.1949318	0.0000	Down
Cd300lf	CD300 molecule like family member F	0.457483	−1.1282103	0.0002	Down
Sbno2	Strawberry notch 2	0.45762	−1.1277768	0.0000	Down
Atp6v0d2	Atpase, H+ transporting, lysosomal V0 subunit D2	0.474209	−1.0764065	0.0168	Down
Atp6v0b	Atpase, H+ transporting, lysosomal V0 subunit B	0.484969	−1.0440367	0.0017	Down
Tcirg1	T cell, immune regulator 1, atpase, H+ transporting, lysosomal V0 protein A3	0.485776	−1.0416378	0.0318	Down
Acp5	Acid phosphatase 5, tartrate resistant	0.488476	−1.0336416	0.0021	Down
Tfrc	Transferrin receptor	0.500787	−0.9977298	0.0170	Down
Socs1	Suppressor of cytokine signaling 1	0.502007	−0.9942197	0.0000	Down
Atp6v0e	Atpase, H+ transporting, lysosomal V0 subunit E	0.503671	−0.9894465	0.0000	Down
Fos	FBJ osteosarcoma oncogene	0.504342	−0.9875268	0.0371	Down
Sirpb1a	Signal-regulatory protein beta 1A	0.504386	−0.9873994	0.0261	Down
Il1r1	Interleukin 1 receptor, type I	0.512523	−0.964311	0.0018	Down
Ctsk	Cathepsin K	0.513274	−0.9621981	0.0071	Down
Nfkb2	Nuclear factor of kappa light polypeptide gene enhancer in B cells 2, p49/p100	0.516089	−0.9543074	0.0001	Down
Gm49339	Predicted gene, 49339	0.528553	−0.9198802	0.0093	Down
Fosl2	Fos-like antigen 2	0.530645	−0.9141807	0.0000	Down
Relb	Avian reticuloendotheliosis viral (v-rel) oncogene related B	0.533646	−0.9060441	0.0001	Down
Pparg	Peroxisome proliferator-activated receptor gamma	1.969141	0.97756671	0.0197	Up
Trf	Transferrin	2.100132	1.07047982	0.0177	Up
Map2k6	Mitogen-activated protein kinase kinase 6	2.434473	1.2836092	0.0000	Up
Gpc3	Glypican 3	2.597385	1.37705978	0.0011	Up

FC, fold change; MM, medium-dose MAI group; MO, CIA model group; CIA, collagen-induced arthritis; MAI, melittin acupoint injection.

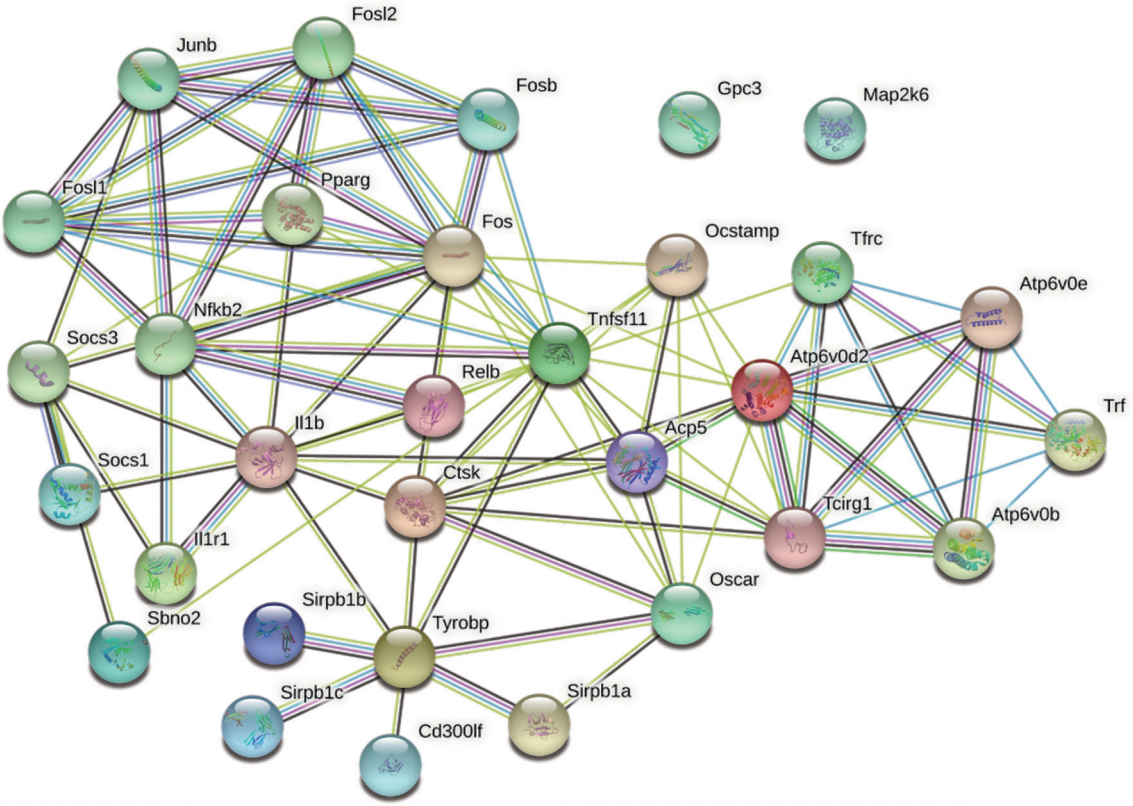

Figure 6 Protein network interaction analysis of differentially expressed genes in the osteoclast differentiation pathway in the CIA mice. CIA, collagen-induced arthritis.

RA bone destruction is mainly related to abnormal bone resorption caused by excessive osteoclast activation (36,37).

Immune factors play a pivotal role in osteoclast differentiation and expression. TNF-α and IL-6 are major proinflammatory cytokines in RA. IL-6 can promote osteoclast formation via inducing RANKL or directly stimulating osteoclast precursors (35). TNF-α not only inhibits bone formation but can also promote osteoclasts by inducing RANKL and directly stimulating osteoclast precursors through TNF receptor 1 (6,38). As anti-inflammatory factors, IL-4 and IL-10 suppress osteoclast formation (39,40). A study found that naringenins inhibited RANKL-induced osteoclastogenesis and osteoclast bone resorption by promoting the release of IL-4 from T cells (41). Notably, Gao *et al.* also confirmed that IL-10 binds to signal transducer and activator of transcription 1 (STAT1) through maternally expressed gene 3 (MEG3) and further regulates interferon regulatory factor 8 (IRF8) expression, thereby affecting osteoclast differentiation and wear particle-induced osteolysis (42). Similarly, we also showed that the more severe the joint bone destruction is, the higher the serum levels of TNF-α and IL-6, yet the lower the levels of IL-4 and IL-10 are compared with the other groups. All these results indicated that both anti-inflammatory and pro-inflammatory factors were closely related to osteoclast formation and thus affected the progression of bone destruction.

As a bridge between the immune system and the skeletal system (43), RANKL is a key cytokine for inducing osteoclasts (44,45). When RANKL combines with RANK, it induces the trimerization of RANK and tumor necrosis factor receptor-associated factors 6 (TRAF6), thereby activating NF-κB, mitogen-activated protein kinase (MAPK), and other pathways (46). According to the contents of the KEGG database (https://www.genome.jp/kegg/), osteoclast differentiation mainly includes the NF-κB, MAPK, phosphatidylinositol-3-kinase (PI3K)-protein kinase B (PKB or Akt), Janus kinase (JAK)-STAT, and calcium signaling pathways. Activation of the NF-κB signaling pathway has been shown to be fatal in osteoclastogenesis,

which can be induced by RANKL (47,48). A previous study showed that melittin enhances apoptosis by inhibiting NF-κB and STAT3 activation and B-cell lymphoma 2 (Bcl-2) expression in human fibroblast-like synoviocytes in RA induced by the IL-6-sIL-6R complex (49). The activation of NF-κB depends on both classical and alternative pathways (50). The alternative pathway proceeds via phosphorylation and proteolytic processing of NF-κB2 (p100) and the subsequent activation of heterodimer RelB/NF-κB2 (p52). More specifically, NF-κB-inducing kinase (NIK) stability is destabilized by combined TRAF3 under normal conditions. However, activation of receptor subsets through the TNFR superfamily (such as RANK) and lymphotoxin-βR causes TRAF proteins (including TRAF3) to be recruited into the receptor. When TRAF3 is inactivated (probably by degradation or sequestration), the active NIK is thus released. Subsequently, NIK phosphorylates and activates I kappa-B kinase alpha (IKKα) homodimer. IKKα phosphorylates p100 to induce processing to p52; p52 combines with RelB and then produces the RelB/p52 heterodimer, which migrates to the nucleus (51,52). Our study found that the *NF-κB2* and *RelB* genes are downregulated, and belong to the nonclassical NF-κB pathway.

The NF-κB pathway contributes to the induction and activation of Fos and subsequent nuclear factor of activated T cells 1 (NFATc1) induction (53). The downstream Fos family proteins (c-Fos, FosB, Fra-1, and Fra-2) form the activating protein-1 (AP-1) complex with the Jun family proteins (c-Jun, JunB, and JunD) and play a key role in osteoclast differentiation (54,55). Together with NFATc1 and other transcription factors, AP-1 can directly induce the expression of a variety of osteoclast-specific genes, such as *CTSk*, *TRAP*, and *OSCAR*, to achieve osteoclast differentiation (47,56,57). In our study, we found that MAI treatment decreased the RANKL, CTSK, OSCAR, OCSTAMP, and AP-1 at the gene level, while minimizing the osteoclast expression of the ankle in CIA mice. This supports its effectiveness in alleviating bone destruction in RA.

Conclusions

MAI can inhibit the inflammation of arthritis and the RANKL/NF-kB pathway to reduce osteoclast generation, thereby inhibiting bone destruction in CIA mice and exerting osteoprotective effects. MAI simultaneously has the triple effects of melittin, acupoint function, and needling. However, this study also had some limitations, such as whether MAI can affect osteoblasts and further alter the balance between osteoblasts and osteoclasts on bone destruction, a relationship which should be investigated in additional research.

Acknowledgments

Funding: This research was supported by the Traditional Chinese Medicine Bureau of Guangdong Province (No. 20202120) and National Natural Science Foundation of China (No. 81873382).

Footnote

Reporting Checklist: The authors have completed the ARRIVE reporting checklist. Available at https://qims.amegroups.com/article/view/10.21037/qims-23-254/rc.

Conflicts of Interest: All authors have completed the ICMJE uniform disclosure form (available at https://qims.amegroups.com/article/view/10.21037/qims-23-254/coif). The authors have no conflicts of interest to declare.

Ethical Statement: The authors are accountable for all aspects of the work in ensuring that questions related to the accuracy or integrity of any part of the work are appropriately investigated and resolved. Animal experiments were performed under a project license (No. SMUL2022024) granted by the Ethics Committee of Southern Medical University, in compliance with Southern Medical University guidelines for the care and use of animals.

References

1. Sparks JA. Rheumatoid Arthritis. Ann Intern Med 2019;170:ITC1-ITC16.
2. Smolen JS, Aletaha D, McInnes IB. Rheumatoid arthritis.

Lancet 2016;388:2023-38.
3. Otón T, Carmona L. The epidemiology of established rheumatoid arthritis. Best Pract Res Clin Rheumatol 2019;33:101477.
4. Kougkas N, Dara A, Pagkopoulou E, Dimitriadou A, Papadimitriou E, Avdelidou E, Garyfallos A, Dimitroulas T. Methotrexate induced neurotoxicity in a patient with rheumatoid arthritis on rituximab therapy: a case-based review. Rheumatol Int 2022;42:1849-54.
5. Hazlewood GS, Schieir O, Bykerk V, Mujaab K, Tugwell P, Wells G, Richards D, Proulx L, Hull PM, Bartlett SJ. Frequency of Symptomatic Adverse Events in Rheumatoid Arthritis: An Exploratory Online Survey. J Rheumatol 2022;49:998-1005.
6. Schett G, Gravallese E. Bone erosion in rheumatoid arthritis: mechanisms, diagnosis and treatment. Nat Rev Rheumatol 2012;8:656-64.
7. Walsh NC, Gravallese EM. Bone remodeling in rheumatic disease: a question of balance. Immunol Rev 2010;233:301-12.
8. Chen J, Guan SM, Sun W, Fu H. Melittin, the Major Pain-Producing Substance of Bee Venom. Neurosci Bull 2016;32:265-72.
9. Wehbe R, Frangieh J, Rima M, El Obeid D, Sabatier JM, Fajloun Z. Bee Venom: Overview of Main Compounds and Bioactivities for Therapeutic Interests. Molecules 2019;24:2997.
10. Du G, He P, Zhao J, He C, Jiang M, Zhang Z, Zhang Z, Sun X. Polymeric microneedle-mediated transdermal delivery of melittin for rheumatoid arthritis treatment. J Control Release 2021;336:537-48.
11. Shin JM, Jeong YJ, Cho HJ, Park KK, Chung IK, Lee IK, Kwak JY, Chang HW, Kim CH, Moon SK, Kim WJ, Choi YH, Chang YC. Melittin suppresses HIF-1α/VEGF expression through inhibition of ERK and mTOR/p70S6K pathway in human cervical carcinoma cells. PLoS One 2013;8:e69380.
12. Bae S, Gu H, Gwon MG, An HJ, Han SM, Lee SJ, Leem J, Park KK. Therapeutic Effect of Bee Venom and Melittin on Skin Infection Caused by Streptococcus pyogenes. Toxins (Basel) 2022.
13. Aghighi Z, Ghorbani Z, Moghaddam MH, Fathi M, Abdollahifar MA, Soleimani M, Karimzadeh F, Rasoolijazi H, Aliaghaei A. Melittin ameliorates motor function and prevents autophagy-induced cell death and astrogliosis in rat models of cerebellar ataxia induced by 3-acetylpyridine. Neuropeptides 2022;96:102295.
14. Fan KJ, Li YW, Wu J, Wang QS, Xu BX, Teng H, Chen SJ, Wang TY. Pharmacology and molecular docking study of cartilage protection of Chinese herbal medicine Fufang Shatai Heji (STHJ) by inhibiting the expression of MMPs in collagen-induced arthritis mice. Ann Palliat Med 2022;11:466-79.
15. Sha T, Gao LL, Zhang CH, Zheng JG, Meng ZH. An update on acupuncture point injection. QJM 2016;109:639-41.
16. Zhai Y, Yu W, Shen W. Diffusion Tensor Imaging Evaluates Effects of Acupoint Injection at Zusanli (ST36) for Type 2 Diabetic Peripheral Neuropathy. Med Sci Monit 2022;28:e935979.
17. Liu M, Wang Y, Li N, Cui J, Fan W, Yang S, Li L, Zeng J, Li M. Effects of acupoint injection for stroke patients with hemiplegia: A protocol for systematic review and meta-analysis of randomized controlled trials. Medicine (Baltimore) 2021;100:e28374.
18. Lin TY, Hsieh CL. Clinical Applications of Bee Venom Acupoint Injection. Toxins (Basel) 2020.
19. Ling Y, Yang J, Hua D, Wang D, Zhao C, Weng L, Yue D, Cai X, Meng Q, Chen J, Sun X, Kong W, Zhu L, Cao P, Hu C. ZhiJingSan Inhibits Osteoclastogenesis via Regulating RANKL/NF-κB Signaling Pathway and Ameliorates Bone Erosion in Collagen-Induced Mouse Arthritis. Front Pharmacol 2021;12:693777.
20. Wang Q, Jiang H, Li Y, Chen W, Li H, Peng K, Zhang Z, Sun X. Targeting NF-kB signaling with polymeric hybrid micelles that co-deliver siRNA and dexamethasone for arthritis therapy. Biomaterials 2017;122:10-22.
21. Meng X, Guo X, Zhang J, Moriya J, Kobayashi J, Yamaguchi R, Yamada S. Acupuncture on ST36, CV4 and KI1 Suppresses the Progression of Methionine- and Choline-Deficient Diet-Induced Nonalcoholic Fatty Liver Disease in Mice. Metabolites 2019;9:299.
22. Liu M, Zhou X, Zhou L, Liu Z, Yuan J, Cheng J, Zhao J, Wu L, Li H, Qiu H, Xu J. Carnosic acid inhibits inflammation response and joint destruction on osteoclasts, fibroblast-like synoviocytes, and collagen-induced arthritis rats. J Cell Physiol 2018;233:6291-303.
23. Cai XY, Ge JR, Xu L, Liang FQ, Zhu Y, Tai Y, Zhang XZ, Shu JL, Mei D, Han L, Wang C, Tang XY, Zhang LL, Wei W. Paeoniflorin-6'-o-benzene sulfonate (CP-25) improves vasculitis through inhibiting IL-17A/JAK/STAT3 signaling pathway in endothelial cells of HFD CIA rats. Phytother Res 2021;35:1033-47.
24. Shi L, Zhao Y, Feng C, Miao F, Dong L, Wang T, Stalin A, Zhang J, Tu J, Liu K, Sun W, Wu J. Therapeutic effects of shaogan fuzi decoction in rheumatoid arthritis:

Network pharmacology and experimental validation. Front Pharmacol 2022;13:967164.
25. Lorenzo N, Altruda F, Silengo L, Del Carmen Dominguez M. APL-1, an altered peptide ligand derived from heat-shock protein, alone or combined with methotrexate attenuates murine collagen-induced arthritis. Clin Exp Med 2017;17:209-16.
26. Hayer S, Vervoordeldonk MJ, Denis MC, Armaka M, Hoffmann M, Bäcklund J, Nandakumar KS, Niederreiter B, Geka C, Fischer A, Woodworth N, Blüml S, Kollias G, Holmdahl R, Apparailly F, Koenders MI. 'SMASH' recommendations for standardised microscopic arthritis scoring of histological sections from inflammatory arthritis animal models. Ann Rheum Dis 2021;80:714-26.
27. Kondo Y, Kaneko Y, Sugiura H, Matsumoto S, Nishina N, Kuwana M, Jinzaki M, Takeuchi T. Pre-treatment interleukin-6 levels strongly affect bone erosion progression and repair detected by magnetic resonance imaging in rheumatoid arthritis patients. Rheumatology (Oxford) 2017;56:1089-94.
28. Dar HY, Azam Z, Anupam R, Mondal RK, Srivastava RK. Osteoimmunology: The Nexus between bone and immune system. Front Biosci (Landmark Ed) 2018;23:464-92.
29. Wang Z, Huang W, Ren F, Luo L, Zhou J, Huang D, Jiang M, Du H, Fan J, Tang L. Characteristics of Ang-(1-7)/Mas-Mediated Amelioration of Joint Inflammation and Cardiac Complications in Mice With Collagen-Induced Arthritis. Front Immunol 2021;12:655614.
30. Sobotka AK, Franklin RM, Adkinson NF Jr, Valentine M, Baer H, Lichtenstein LM. Allergy to insect stings. II. Phospholipase A: the major allergen in honeybee venom. J Allergy Clin Immunol 1976;57:29-40.
31. Lee HS, Kim YS, Lee KS, Seo HS, Lee CY, Kim KK. Detoxification of Bee Venom Increases Its Anti-inflammatory Activity and Decreases Its Cytotoxicity and Allergenic Activity. Appl Biochem Biotechnol 2021;193:4068-82.
32. Yang F, Gong Y, Yu N, Yao L, Zhao X, Hong S, Wang S, Chen B, Xu Y, Pang G, Wang H, Guo Y, Li Y, Guo Y, Xu Z. ST36 Acupuncture Alleviates the Inflammation of Adjuvant-Induced Arthritic Rats by Targeting Monocyte/Macrophage Modulation. Evid Based Complement Alternat Med 2021;2021:9430501.
33. Yu N, Yang F, Zhao X, Guo Y, Xu Y, Pang G, Gong Y, Wang S, Liu Y, Fang Y, Yu K, Yao L, Wang H, Zhang K, Liu B, Wang Z, Guo Y, Xu Z. Manual acupuncture at ST36 attenuates rheumatoid arthritis by inhibiting M1 macrophage polarization and enhancing Treg cell populations in adjuvant-induced arthritic rats. Acupunct Med 2023;41:96-109.
34. Okamoto K, Nakashima T, Shinohara M, Negishi-Koga T, Komatsu N, Terashima A, Sawa S, Nitta T, Takayanagi H. Osteoimmunology: The Conceptual Framework Unifying the Immune and Skeletal Systems. Physiol Rev 2017;97:1295-349.
35. Kim JY, Cheon YH, Kwak SC, Baek JM, Yoon KH, Lee MS, Oh J. Emodin regulates bone remodeling by inhibiting osteoclastogenesis and stimulating osteoblast formation. J Bone Miner Res 2014;29:1541-53.
36. Xie Y, Jiang X, Wang P, Zheng X, Song J, Bai M, Tang Y, Fang X, Jia Y, Li Z, Hu F. SR-A neutralizing antibody: potential drug candidate for ameliorating osteoclastogenesis in rheumatoid arthritis. Clin Exp Immunol 2022;207:297-306.
37. Li Y, Yang C, Jia K, Wang J, Wang J, Ming R, Xu T, Su X, Jing Y, Miao Y, Liu C, Lin N. Fengshi Qutong capsule ameliorates bone destruction of experimental rheumatoid arthritis by inhibiting osteoclastogenesis. J Ethnopharmacol 2022;282:114602.
38. Lam J, Takeshita S, Barker JE, Kanagawa O, Ross FP, Teitelbaum SL. TNF-alpha induces osteoclastogenesis by direct stimulation of macrophages exposed to permissive levels of RANK ligand. J Clin Invest 2000;106:1481-8.
39. Jin Q, Yang H, Jing Z, Hong-Hua W, Ben-Jing S, Li-Ting W, Li-Juan Y, Wei X, Xia K, Juan W, Wei Z. IL4/IL4R signaling promotes the osteolysis in metastatic bone of CRC through regulating the proliferation of osteoclast precursors. Mol Med 2021;27:152.
40. Tanaka K, Yamagata K, Kubo S, Nakayamada S, Sakata K, Matsui T, Yamagishi SI, Okada Y, Tanaka Y. Glycolaldehyde-modified advanced glycation end-products inhibit differentiation of human monocytes into osteoclasts via upregulation of IL-10. Bone 2019;128:115034.
41. Wang W, Li M, Luo M, Shen M, Xu C, Xu G, Chen Y, Xia L. Naringenin inhibits osteoclastogenesis through modulation of helper T cells-secreted IL-4. J Cell Biochem 2018;119:2084-93.
42. Gao X, Ge J, Zhou W, Xu L, Geng D. IL-10 inhibits osteoclast differentiation and osteolysis through MEG3/IRF8 pathway. Cell Signal 2022;95:110353.
43. Honma M, Ikebuchi Y, Suzuki H. RANKL as a key figure in bridging between the bone and immune system: Its physiological functions and potential as a pharmacological target. Pharmacol Ther 2021;218:107682.
44. Wada T, Nakashima T, Hiroshi N, Penninger JM. RANKL-RANK signaling in osteoclastogenesis and bone

disease. Trends Mol Med 2006;12:17-25.
45. Sun K, Zhu J, Deng Y, Xu X, Kong F, Sun X, Huan L, Ren C, Sun J, Shi J. Gamabufotalin Inhibits Osteoclastgenesis and Counteracts Estrogen-Deficient Bone Loss in Mice by Suppressing RANKL-Induced NF-κB and ERK/MAPK Pathways. Front Pharmacol 2021;12:629968.
46. Zhi X, Fang C, Gu Y, Chen H, Chen X, Cui J, Hu Y, Weng W, Zhou Q, Wang Y, Wang Y, Jiang H, Li X, Cao L, Chen X, Su J. Guaiacol suppresses osteoclastogenesis by blocking interactions of RANK with TRAF6 and C-Src and inhibiting NF-κB, MAPK and AKT pathways. J Cell Mol Med 2020;24:5122-34.
47. Kavitha CV, Deep G, Gangar SC, Jain AK, Agarwal C, Agarwal R. Silibinin inhibits prostate cancer cells- and RANKL-induced osteoclastogenesis by targeting NFATc1, NF-κB, and AP-1 activation in RAW264.7 cells. Mol Carcinog 2014;53:169-80.
48. Chen H, Fang C, Zhi X, Song S, Gu Y, Chen X, Cui J, Hu Y, Weng W, Zhou Q, Wang Y, Wang Y, Jiang H, Li X, Cao L, Chen X, Su J. Neobavaisoflavone inhibits osteoclastogenesis through blocking RANKL signalling-mediated TRAF6 and c-Src recruitment and NF-κB, MAPK and Akt pathways. J Cell Mol Med 2020;24:9067-84.
49. Kim SK, Park KY, Yoon WC, Park SH, Park KK, Yoo DH, Choe JY. Melittin enhances apoptosis through suppression of IL-6/sIL-6R complex-induced NF-κB and STAT3 activation and Bcl-2 expression for human fibroblast-like synoviocytes in rheumatoid arthritis. Joint Bone Spine 2011;78:471-7.
50. Bakkar N, Guttridge DC. NF-kappaB signaling: a tale of two pathways in skeletal myogenesis. Physiol Rev 2010;90:495-511.
51. Brown KD, Claudio E, Siebenlist U. The roles of the classical and alternative nuclear factor-kappaB pathways: potential implications for autoimmunity and rheumatoid arthritis. Arthritis Res Ther 2008;10:212.
52. Jimi E, Fukushima H. NF-κB signaling pathways and the future perspectives of bone disease therapy using selective inhibitors of NF-κB. Clin Calcium 2016;26:298-304.
53. Tsukasaki M, Takayanagi H. Osteoimmunology: evolving concepts in bone-immune interactions in health and disease. Nat Rev Immunol 2019;19:626-42.
54. Cheng X, Yin C, Deng Y, Li Z. Exogenous adenosine activates A2A adenosine receptor to inhibit RANKL-induced osteoclastogenesis via AP-1 pathway to facilitate bone repair. Mol Biol Rep 2022;49:2003-14.
55. Wagner EF, Matsuo K. Signalling in osteoclasts and the role of Fos/AP1 proteins. Ann Rheum Dis 2003;62 Suppl 2:ii83-5.
56. Pang M, Rodríguez-Gonzalez M, Hernandez M, Recinos CC, Seldeen KL, Troen BR. AP-1 and Mitf interact with NFATc1 to stimulate cathepsin K promoter activity in osteoclast precursors. J Cell Biochem 2019;120:12382-92.
57. Jing W, Feng L, Peng K, Zhang W, Wang B. Formononetin attenuates osteoclast differentiation and calcium loss by mediating transcription factor AP-1 in type I diabetic mice. J Biochem Mol Toxicol 2022;36:e23042.

Cite this article as: Liu F, Chen F, Yang L, Qiu F, Zhong G, Gao S, Xi W, Lai M, He Q, Chen Y, Chen W, Zhang J, Yang L. Melittin acupoint injection in attenuating bone erosion in collagen-induced arthritis mice via inhibition of the RANKL/NF-κB signaling pathway. Quant Imaging Med Surg 2023;13(9):5996-6013. doi: 10.21037/qims-23-254

